Journal of Catalysis 309 (2014) 115–120

Contents lists available at ScienceDirect

Journal of Catalysis

journal homepage: www.elsevier.com/locate/jcat

The structure, electronic, and optical properties of (Sm,N)-codoped anatase TiO_2 photocatalyst: A density functional study

Yanming Lin [a], Zhenyi Jiang [a,*], Ruiqin Zhang [b], Chaoyuan Zhu [c], Xiaoyun Hu [d], Xiaodong Zhang [a], Haiyan Zhu [a]

[a] Institute of Modern Physics, Northwest University, Xi'an 710069, PR China
[b] Department of Physics and Materials Science, City University of HongKong, HongKong
[c] Department of Applied Chemistry, Institute of Molecular Science and Center for Interdisciplinary Molecular Science, National Chiao-Tung University, Hsinchu 30050, Taiwan
[d] Department of Physics, Northwest University, Xi'an 710069, PR China

ARTICLE INFO

Article history:
Received 15 April 2012
Revised 15 July 2013
Accepted 16 July 2013
Available online 17 October 2013

Keywords:
TiO_2
Codoping
Visible-light photocatalyst
Density functional theory

ABSTRACT

The geometrical, electronic, and optical properties of Sm-doped, N-doped, and (Sm,N)-codoped anatase TiO_2 were successfully calculated and simulated using the spin-polarized density functional theory. The researches of geometrical structures show that (Sm,N) codoping leads to lattice distortion, which reduces the recombination of the photogenerated electron–hole pairs. Moreover, the calculated results indicate that the synergistic effects of (Sm,N) codoping can lead to an obvious band gap narrowing and a N 2p state appearing in the forbidden gap, which leads to a significant redshift of the optical absorption edge and enhances the photocatalytic activity of the (Sm,N)-codoped anatase TiO_2.

1. Introduction

Titanium dioxide (TiO_2) has been extensively studied in the past few years for being extremely useful in many technological applications. It is one of the most promising photocatalysts for environmental clean up, photogeneration of hydrogen from water, and solar energy utilization [1,2]. However, its wide band gap (3.2 eV for the anatase structure [3]) leads to a low photon utilization efficiency of sunlight because only the ultraviolet-light ($\lambda < 400$ nm) can afford the energy for the electron transition from the valence band (VB) to the conduction band (CB) [4,5]. Furthermore, the quantum yield is low due to rapid recombination between excited electrons and holes [6]. Therefore, to enhance the photocatalytic activity of TiO_2, extending optical absorption range of TiO_2 into visible-light region and reducing the recombination of excited electron–hole (e^+–h^-) pairs are two main subjects for the increased utility of TiO_2.

An effective approach to extend the TiO_2 optical absorption edge into visible-light region and reduce the photogenerated electron–hole pairs recombination rate is doping the TiO_2 with transition-metal (TM) or non-metal elements. The TM element doping can effectively lower the electron–hole pairs recombination rate, which promotes the photocatalytic efficiency and extends optical response from ultraviolet to visible region. For example, Dholam et al. reported hydrogen production by photocatalytic water-splitting using Cr- or Fe-doped TiO_2 composite thin films photocatalyst [7]. Li et al. studied photocatalytic activity of nanoglued Sn-doped TiO_2, the results suggested that an appropriate amount of Sn dopant could greatly increase the amount of hydroxyl radicals generated by TiO_2 nanoparticles, which were responsible for the obvious increase in photocatalytic activity [8]. Lin et al. investigated visible-light photocatalytic activity of Ni-doped TiO_2 from *ab initio* calculations, the calculated results indicated that substitutionally Ni to O-doped anatase and rutile TiO_2 had a series of impurity energy levels appearing in the forbidden gap, which may be responsible for the redshift of optical absorption edge and visible-light photocatalytic activity in Ni-doped TiO_2 [9]. Chiou et al. examined photocatalytic degradation of phenol in aqueous solutions by Pr-doped TiO_2 nanoparticles [10]. The Pr-doped TiO_2 exhibited high activity for photocatalytic degradation of phenol in the experiment, which was due to the presence of Pr ions in the TiO_2 nanoparticles causing a significant absorption shift toward the visible-light region. For non-metal elements doping, the doping of N [11–14], C [15–18], Si [19,20], S [21,22], B [23], and P [24] in TiO_2 can reduce its band gap and shift its optical absorption edge into visible-light region because the related impurity states are near the valence band edge, which can minimize their possibility as recombination centers compared to transition-metal doping. Moreover, some scientists attempt to improve the photocatalytic

* Corresponding author. Fax: +86 29 88302331.
E-mail addresses: linymnwu@gmail.com (Y. Lin), jiangzy@nwu.edu.cn (Z. Jiang).

0021-9517/$ - see front matter © 2013 Elsevier Inc. All rights reserved.
http://dx.doi.org/10.1016/j.jcat.2013.07.016

of TiO_2 by TM and non-metal elements codoped approach. Tan et al. investigated visible-light absorption and photocatalytic activity of Mo- and N-codoped TiO_2, and found the codoped sample exhibits better absorption performance than monodoped sample in visible-light region [25]. Jia et al. found the mixing of O 2p, N 2p, S 3p, and Ti 3d states in the forbidden gap of (N,S)-codoped TiO_2, which can result in the higher visible-light photocatalytic activities than those monodoped TiO_2 [26]. Lin et al. reported synergistic effects of Eu/Si codoping can effectively extend the optical absorption edge [27]. These results indicate that codoping with TM and non-metal elements is one of the most effective approaches to extend the absorption edge to the visible-light range in anatase TiO_2. In addition, We recognize that the DFT + U methodology has successfully been applied to TiO_2 system including the setting of the U-parameter and the calculation of optical adsorption for defective systems [28–34]. For example, Morgan et al. used the DFT + U to study the formations of intrinsic n-type defects and calculated optical absorption spectra for all defects in TiO_2 material [28]. Jia et al. investigated the electronic and optical properties of (N,Fe)-codoped anatase TiO_2 photocatalyst by the DFT + U method [30]. Zhang et al. studied the effect of substitutional N, Ce, and Ce + N doping on the electronic structure and optical properties of anatase TiO_2 with the DFT + U approach [33].

Recently, visible-light induced (Sm,N)-codoped TiO_2 photocatalysts have been successfully synthesized by Ma et al. [35]. They show that N doping can extend the optical absorption edge to visible-light region, and the doping of Sm into TiO_2 can efficiently inhibit the recombination of electrons-holes pairs. The (Sm,N)-codoped TiO_2 sample presents much higher photocatalytic activity than N-doped TiO_2 and pure TiO_2 under visible-light irradiation. However, to the best of our knowledge, there has been no report on the geometrical, electronic, and optical properties of (Sm,N)-codoped anatase TiO_2. Therefore, the physical and chemical origin of the enhanced photocatalytic activity and the longer wavelength optical absorption remains unexplained.

In the present work, the electronic and optical properties of (Sm,N)-codoped anatase TiO_2 have been investigated using the density functional theory (DFT) to reveal the microscopic mechanism for band gap narrowing and the origin of the enhanced photocatalytic activity. For comparison, the corresponding calculation and theoretic analysis are also conducted for pure, Sm- and N-doped anatase TiO_2. Our theoretical analysis provides a probable explanation for the experimental work of Ma et al. We also discuss the thermodynamic properties of Sm-, N-, and (Sm,N)-codoped TiO_2 by analysis of the calculated formation energies.

2. Computational details

All of the spin-polarized calculations were performed using the projector augmented wave (PAW) pseudopotentials as implemented in the VASP code [36,37]. The exchange correlation potential was treated by the generalized gradient approximation (GGA) with the Perdew–Wang parameterization (known as GGA-PW91) [38]. The Brillouin-zone integrations were approximated by using the special k-point sampling of the Monhkorst–Pack scheme [39]. A cutoff energy of 500 eV and a mesh size of $5 \times 5 \times 5$ were used for geometry optimization and electronic structure calculations. Using the block Davidson scheme, both the atomic positions and cell parameters were optimized until the residual forces were below 0.01 eV/Å. It was well-known that the traditional DFT method usually underestimated the band gap for semiconductors. However, the DFT + U approach introduced an on-site correction in order to describe systems with localized d and f electrons, which can produce better band gaps in comparison with experimental results. Therefore, our all calculations of the electronic and optical properties were conducted using the GGA + U method [40–43] for both Ti 3d and Sm 4f electrons. It was found that the band gap of pure anatase TiO_2 was 2.9 eV with U = 10.0 eV and J = 1.0 eV for Ti 3d electrons, and was only weakly dependent on J value. This accords well with the experimental value of 3.2 eV [44].

The valence electron configurations which included Ti ($3d^2 4s^2$), O ($2s^2 2p^4$), Sm ($4f^6 5s^2$) and N ($2s^2 2p^3$) were considered in this study. All the doped systems were constructed from a relaxed ($2 \times 2 \times 1$) 48-atom anatase TiO_2 supercell (see Fig. 1). A variety of possible doping model were considered, such as substitutional Sm at the Ti site (Sm@Ti), substitutional Sm at the O site (Sm@O), substitutional N at the Ti site (N@Ti), and substitutional N at the O site (N@O) for the bulk doped systems. For codoped systems, Sm locates either at Ti or at O and N locates either at O or at Ti, such as Sm@Ti&N@Ti, Sm@O&N@O, Sm@Ti&N@O, and Sm@O&N@Ti.

3. Results and discussion

3.1. Geometry analysis

Anatase has a tetragonal crystal structure with space group $I_{41/amd}(141)$. The unit cell contains four TiO_2 formula units. We performed structure optimization for pure anatase TiO_2 supercell. The calculated lattice parameters of pure TiO_2 model are $a = b = 3.816$ Å and $c = 9.618$ Å at ambient conditions, which are in good agreement with the experiment value of $a = b = 3.782$ Å and $c = 9.502$ Å within 1.2%, respectively [44]. These results indicate that our calculation methods are reasonable, and the calculated results are authentic.

The average bond lengths of the doping TiO_2 after geometry optimization are summarized in Table 1. For pure anatase TiO_2, the average Ti–O bond length is 1.977 Å, there is no significant change compared with that of the Sm- and N-doped one. However, the average Ti–O bond lengths of the (Sm,N)-codoped TiO_2 in the supercell is shorter than Sm- and N-doped TiO_2. The average Ti–Sm bond length in Sm-doped and (Sm,N)-codoped systems are longer than the Ti–O bond length as the radius of Sm atom is larger than that of O atom. Due to the larger radius of N, the average Ti–N bond length of N-doped and (Sm,N)-codoped TiO_2 is also longer than that of the Ti–O bond. In the case of codoped TiO_2, the length of all these bonds is increased. The results show that (Sm,N)-codoping leads to a significant lattice distortion and a high defect formation energy, which in turn changes the dipole moments, makes the separation of photogenerated electrons and holes easier.

3.2. Defect formation energies

To study the relative stability of Sm-doped, N-doped, and (Sm,N)-codoped anatase TiO_2 systems, we have calculated the defect formation energy (E_f), which is defined by the expression,

$$E_{f(X@Y)} = E_{(X@Y)} - E_{(\text{pure})} - (\mu_X - \mu_Y) \quad (1)$$

$$E_{f(\text{Sm@Y\&N@Y})} = E_{(\text{Sm@Y\&N@Y})} - E_{(\text{pure})} - (\mu_{\text{Sm}} + \mu_{\text{N}} - \mu_Y - \mu_Y) \quad (2)$$

$$(X = \text{Sm}, \text{N}; Y = \text{Ti}, \text{O})$$

where $E_{(\text{pure})}$ is the total energy of the pure anatase TiO_2 supercell, $E_{(X@Y)}$ and $E_{(\text{Sm@Y\&N@Y})}$ are the total energy of the monodoped and codoped systems, respectively. Under equilibrium conditions, the concentration of a point defect is controlled by its formation energy, which depends on the chemical potentials of the host and impurity atoms. For TiO_2, the chemical potentials of O and Ti satisfy the relationship $\mu_{\text{Ti}} + 2\mu_{\text{O}} = \mu_{\text{TiO}_2}$, $\mu_{\text{O}} \leqslant \mu_{\text{O}_2/2}$, and $\mu_{\text{Ti}} \leqslant \mu_{\text{Ti}}^{\text{metal}}$. The chemical potential μ_{O} is determined by the energy of an O_2 molecule in the O-rich growth condition (corresponding to a high value of μ_{O}). By referencing μ_{O} to the energy of an O atom in the O_2 molecule, μ_{Ti} in the Ti-rich condition (corresponding to a high value of μ_{Ti})

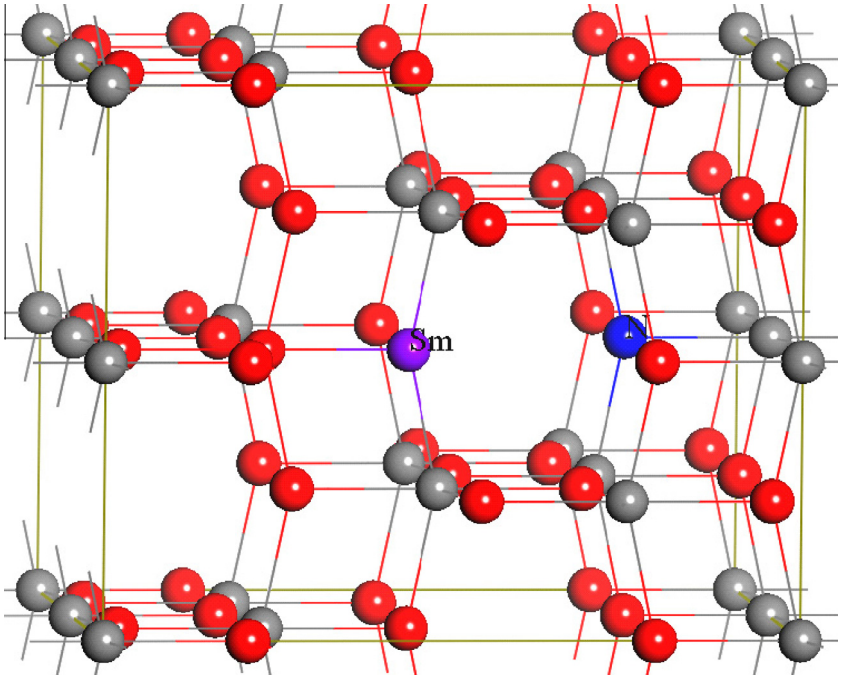

Fig. 1. 48-atom supercell model for defective anatase TiO_2 shows the location of the dopants. The atom doping sites are marked with Sm and N. The gray spheres and red spheres represent the Ti and O atoms, respectively. The purple sphere and blue sphere represent Sm and N atom, respectively.

Table 1
Average bond lengths of the doped TiO_2 after geometry optimization (in Å).

Bond length (Å)	Pure TiO_2	Sm-doped	N-doped	(Sm,N)-codoped
Ti–O	1.977	1.956	1.962	1.937
Ti–N	–	–	2.033	2.232
Ti–Sm	–	2.542	–	2.635
Sm–N	–	–	–	3.072

amounts to the energy of one Ti atom in bulk Ti. μ_{Sm} and μ_N are the chemical potential of Sm and N impurity, which are calculated from bulk Sm and N_2 molecule, respectively. And the calculated chemical potentials for Ti atom, O atom, Sm atom, N atom, and TiO_2 formula unit are listed in Table 2.

Our calculations for a variety of possible configurations of Sm, N locating at different positions in the TiO_2 supercell gave a successful explanation, and the ion of the dopant may be dependent on the growth condition. It should be noted that the smaller the E_f value is the easier to incorporate impurity ions into TiO_2 supercell. Our calculated formation energies for all of doped and codoped TiO_2 systems were summarized in Table 3. It can be observed that the formation energy of Sm@O is much smaller than that of Sm@Ti under both Ti-rich and O-rich growth conditions in Sm-doped TiO_2, indicating that easier replacement of O atom with Sm atom under both Ti-rich and O-rich growth conditions. For N-doped TiO_2, our calculations indicate that the formation energy of N@O is still lower than that of N@Ti under the Ti-rich and O-rich growth conditions, it is indicated that easier replacement of O atom with N atom under the Ti-rich and O-rich growth conditions. In particular,

Table 2
The chemical potentials of Ti, O, Sm, N, and TiO_2 formula unit (in eV).

Ti-rich		O-rich		μ_{Sm}	μ_N	μ_{TiO_2}
μ_{Ti}	μ_O	μ_{Ti}	μ_O			
−2.3970	−9.5448	−4.3197	−12.8472	−3.3000	−7.6762	−21.4866

Table 3
Defect formation energies of doped and codoped anatase TiO_2 systems (in eV).

Doped models		Defect formation energy (eV)	
		Ti-rich	O-rich
Doped	Sm@Ti	9.0242	7.1015
	Sm@O	3.7553	0.4529
	N@Ti	16.1896	14.2669
	N@O	0.1146	−3.1878
Codoped	Sm@Ti&N@Ti	21.2810	17.4356
	Sm@O&N@O	0.6382	−5.9666
	Sm@Ti&N@O	8.5339	3.3088
	Sm@O&N@Ti	13.2528	8.0277

under the O-rich growth condition, the formation energy of N@O is negative, indicating that the N impurity is readily incorporated into the crystal.

For (Sm,N)-codoped TiO_2 systems (see Table 3), the formation energy of Sm@O&N@O codoped model is much smaller than that of the other codoped systems under both Ti-rich and O-rich growth conditions. In particular, under the O-rich growth condition, the formation energy of Sm@O&N@O is negative, indicating that the Sm and N impurities are readily incorporated into the crystal. These results indicate that Sm and N impurities are preferred to substitute the O atoms under both Ti-rich and O-rich growth conditions. To study the two dopants together the effect of their relative positions on the calculated formation energies, we have calculated the defect formation energy of (Sm,N)-codoped anatase TiO_2 using the 216-atom ($3 \times 3 \times 2$) anatase supercell for the different distance of between Sm and N atoms, and the calculated results are listed in Table 4. We can see clearly that the defect formation energy increases gradually with the increase in the distance of between the Sm and N impurity atoms. This indicates that the Sm and N codoping structure is the most stable when the distance of between Sm and N atoms is 3.047 Å. Therefore, the relative position of Sm and N atoms is reasonable in our calculations of the electronic and optical properties.

Table 4
Calculated the defect formation energy of (Sm,N)-codoped anatase TiO_2 with respect to the different distance of between Sm and N atoms.

Distance of Sm and N atoms (Å)	Defect formation energies (eV) (Sm,N)-codoped anatase TiO_2 (Sm@O&N@O)
3.047	−4.8081
4.123	−2.6746
6.669	−3.7840
8.660	−3.3688
11.287	−2.8386

Table 5
The band gap and defect formation energy as a function of *U* values.

U (eV)	Band gap (eV)	Defect formation energy (eV) (Sm,N)-codoped anatase TiO_2 (Sm@O&N@O)	
		Ti-rich	O-rich
3.0	2.326	−70.2499	−76.8547
5.0	2.585	−48.4523	−55.0571
7.0	2.848	−27.9032	−34.5080
9.0	2.879	−8.4642	−15.0690
10.0	2.899	0.6382	−5.9666
11.0	3.638	9.4605	2.8557
12.0	3.902	17.8024	11.1976
15.0	4.217	40.4521	33.8473

In addition, to choose an appropriate *U* parameter using the DFT + *U* approach in TiO_2 system, we have calculated the band gap of anatase TiO_2 about the different *U* parameter, and we have also calculated the defect formation energies of (Sm,N)-codoped anatase TiO_2 for different *U* parameter. Our calculated results are shown in Table 5. It is well-known that one of the most common approaches to determine the appropriate *U* value is to compare the calculated band gap for a set of *U* values with the experimental band gap (3.2 eV). As seen from the Table 5, the band gap of 2.899 eV (≈2.9 eV) is the best close to experimental value, and the band gap of anatase TiO_2 and defect formation energy are increased with the increase in the *U* value.

3.3. Electronic properties

To investigate the electronic properties of codoped anatase TiO_2, the total density of states (TDOS) and partial density of states (PDOS) were calculated by the GGA + *U* approach and plotted in Fig. 2 for all the undoped and doped systems with up-spin DOS above zero and down-spin DOS below zero. For pure anatase TiO_2, the valence band (VB) is mainly contributed by the O 2p state, while the conduction band (CB) is mainly contributed by the Ti 3d state, as shown in Fig. 2a and a′. The calculated band gap value is 2.9 eV for pure anatase TiO_2, which is similar to other theoretical results [45,46]. For Sm-doped (Sm@O) TiO_2 (see Fig. 2b and b′), some gap states mix with the valence band edge and the conduction band edge, and further PDOS analysis shows that the gap states mostly comprise the Sm 4f states, which is due to interaction of between O 2p, Ti 3d states and Sm 4f states. Hence, the photon excitation energy from the VB to the CB has a decrease about 0.8 eV, and thus a redshift of the optical absorption edge is expected in Sm-doped anatase TiO_2. For N-doped (N@O) TiO_2 (see Fig. 2c and c′), substitution of N at the O site acts as a single acceptor due to N having one less electron than O, leading to acceptor N 2p states located above the valence band maximum (VBM) of TiO_2. However, the VBM and the conduction band minimum (CBM) of N-doped TiO_2 exhibit no change with respect to the undoped case. In this case, the gap state (N 2p state) is responsible for photocatalytic activity under visible-light irradiation. However, this gap state can act as a recombination center of electron–hole pairs to limit the efficiency of N-doped TiO_2 in the visible-light region.

For (Sm,N)-codoped (Sm@O&N@O) anatase TiO_2, it is shown clearly in Fig. 2d and d′, four different configurations of Sm@Ti&N@Ti, Sm@O&N@O, Sm@Ti&N@O, and Sm@O&N@Ti were calculated according to doping position. The calculations find that the defect formation energy of Sm@O&N@O model is the lowest. The VBM of (Sm,N)-codoped anatase TiO_2 has an obvious rise about 0.5 eV compared with that of the pure anatase TiO_2 while the con-

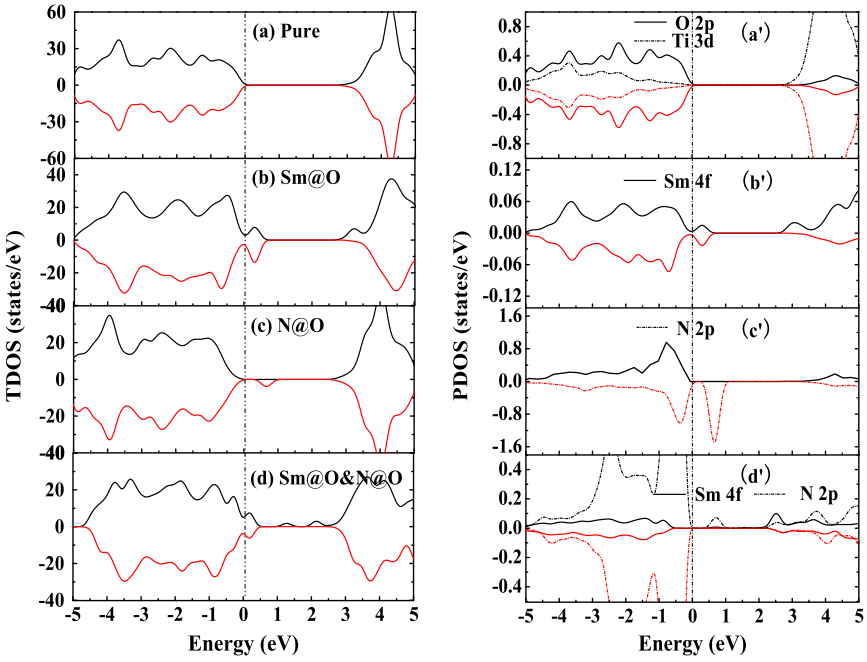

Fig. 2. Calculated TDOS and PDOS of (a and a′) pure anatase TiO_2, (b and b′) Sm-doped TiO_2, (c and c′) N-doped TiO_2, and (d and d′) (Sm,N)-codoped TiO_2. The top of the valence band of pure anatase TiO_2 is taken as the reference level. Curves above and below the horizontal axis refer to the up-spin and down-spin DOS, respectively.

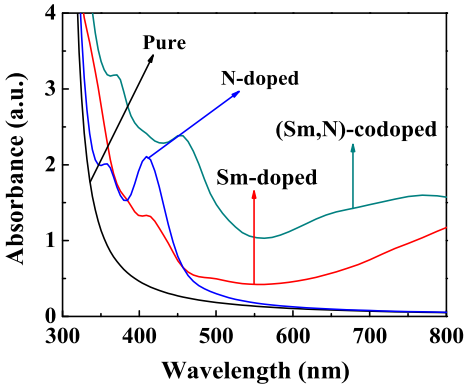

Fig. 3. The optical absorption spectrum of pure and doped anatase TiO_2 systems.

duction band bottom has also a significant decline about 0.3 eV, which is due to the overlap of N 2p and O 2p states and the overlap of Sm 4f and Ti 3d states. In addition, there are two impurity states located in the band gap, which may be due to stronger interactions between the Sm 4f and N 2p orbitals. Therefore, the synergistic effect of (Sm,N) codoping can lead to a decrease in the photon excitation energy and an obvious redshift of the optical absorption edge. The calculated result gives a good explanation for experimental optical absorption broadening to longer wavelength in (Sm,N)-codoped TiO_2.

3.4. Optical properties

For optical properties, it is well-known that the optical absorption is a surface property for the crystal of anatase TiO_2. However, it is reasonable that the effect of doping on electronic structure and optical absorption properties of anatase TiO_2 are investigated by the bulk anatase TiO_2 [47,48], which can partially reflect some experimental results. According to the obtained electronic structures, we calculated the complex dielectric function $\xi = \xi_1 + i\xi_2$. The corresponding optical absorption spectrum was estimated by the following formula

$$I(\omega) = 2\omega\left(\frac{(\xi_1^2(\omega)+\xi_2^2(\omega))^{1/2}-\xi_1(\omega)}{2}\right)^{1/2} \quad (3)$$

where I is the optical absorption coefficient, ω is the angular frequency ($E = \hbar\omega$).

The optical absorption spectrum of the pure and doped anatase TiO_2 systems are calculated, as shown in Fig. 3. It is found that pure anatase TiO_2 can only respond to the ultraviolet-light and shows no absorption performance in the visible-light region. For Sm-doped TiO_2 system, it exhibits good optical absorption property in the visible-light region. Because Sm-doped TiO_2 has a narrowing band gap, it leads to a higher optical absorption performance than pure anatase TiO_2 in long wavelength range, which is consistent with experimental optical absorption spectrum [35]. However, it is clear that the incorporation of N into the TiO_2 lattice induces the increasing optical absorption in the partial visible-light region ($\lambda < 510$ nm) and near ultraviolet-light region, corresponding to a photo transition energy of 2.43 eV from the impurity states (N 2p) to the CB. For (Sm,N)-codoped TiO_2 system, it is interesting that the absorption of ultraviolet- and visible-light are greatly enhanced, which is because that the synergistic effect of (Sm,N) codoping can lead to a decrease in the photon excitation energy in the view of electronic structure. This results may be responsible for the outstanding photocatalytic activity and an obvious redshift of optical absorption edge in (Sm,N)-codoped TiO_2.

4. Conclusion

We have investigated the geometrical, electronic and optical properties of pure, Sm-doped, N-doped, and (Sm,N)-codoped bulk anatase TiO_2 by means of spin-polarized DFT calculations based on plane-wave pseudopotential method. The calculated results indicate that (Sm,N) codoping leads to lattice distortion, which changes the dipole moments and makes the separation of the photogenerated electron–hole pairs easier. In addition, Sm doping leads to an obvious band gap narrowing, and N doping can induce a N 2p state to appear in the forbidden gap. The synergistic effects of (Sm,N) codoping may further reduce the photon excitation energy from the VB to the CB under the visible-light irradiation, which leads to a significant redshift of optical absorption edge and enhances the photocatalytic activity. This results suggest that the (Sm,N)-codoped TiO_2 is a highly active photocatalyst for efficient visible-light photocatalysis.

Acknowledgments

Yanming Lin would like to thank Dr. Kesong Yang and Dr. Run Long for helpful discussions. This work was supported by the National Natural Science Foundation of China under Grants (Nos. 10647008, 50971099 and 21176199), the Research Fund for the Doctoral Program of Higher Education (Nos. 20096101110017 and 20096101110013), Key Project of Natural Science Foundation of Shaanxi Province of China (Nos. 2010JZ002 and 2011JM1001), and Graduate's Innovation Fund of Northwest University of China (No. YZZ12082).

References

[1] R. Asahi, T. Morikawa, T. Ohwaki, K. Aoki, Y. Taga, Science 293 (2001) 269.
[2] C. Burda, Y. Lou, X. Chen, A.C.S. Samia, J. Stout, J.L. Gole, Nano Lett. 3 (2003) 1049.
[3] H. Tang, F. Lévy, H. Berger, P.E. Schmid, Phys. Rev. B 52 (1995) 7771.
[4] O. Carp, C.L. Huisman, A. Reller, Solid State Chem. 32 (2004) 33.
[5] A. Fujishima, T.N. Rao, D.A. Tryk, J. Photochem. Photobiol. C 1 (2000) 1.
[6] Y. Gai, J. Li, S.S. Li, J.B. Xia, S.H. Wei, Phys. Rev. Lett. 102 (2009) 036402.
[7] R. Dholam, N. Patel, M. Adami, A. Miotello, Int. J. Hydrogen Energy 34 (2009) 5337.
[8] X. Li, R. Xiong, G. Wei, J. Hazard. Mater. 164 (2009) 587.
[9] Y.M. Lin, Z.Y. Jiang, C.Y. Zhu, X.Y. Hu, X.D. Zhang, J. Fan, Mater. Chem. Phys. 133 (2012) 746.
[10] C. Chiou, R. Juang, J. Hazard. Mater. 149 (2007) 1.
[11] T. Morikawa, R. Asahi, T. Ohwaki, K. Aoki, Y. Taga, Jpn. J. Appl. Phys. 40 (2001) L561.
[12] S. Livraghi, M.C. Paganini, E. Giamello, A. Selloni, C. Di Valentin, G. Pacchioni, J. Am. Chem. Soc. 128 (2006) 15666.
[13] M. Batzill, E.H. Morales, U. Diebold, Phys. Rev. Lett. 96 (2006) 026103.
[14] Y. Cong, J. Zhang, F. Chen, M. Anpo, J. Phys. Chem. C 111 (2007) 6976.
[15] J.H. Park, S. Kim, A.J. Bard, Nano Lett. 6 (2006) 24.
[16] C. Lettmann, K. Hildenbrand, H. Kisch, W. Wacyk, W.F. Maier, Appl. Catal. B: Environ. 32 (2001) 215.
[17] S.H. Wang, T.K. Chen, K.K. Rao, M.S. Wong, Appl. Catal. B: Environ. 76 (2007) 328.
[18] J. Lu, Y. Dai, M. Guo, L. Yu, K. Lai, B. Huang, Appl. Phys. Lett. 100 (2012) 102114.
[19] R. Jin, Z. Wu, Y. Liu, B. Jiang, H. Wang, J. Hazard. Mater. 161 (2009) 42.
[20] K. Yang, Y. Dai, B. Huang, Chem. Phys. Lett. 456 (2008) 71.
[21] J.C. Yu, W.K. Ho, J.G. Yu, H.Y. Yip, P.K. Wong, J.C. Zhao, Environ. Sic. Technol. 39 (2005) 1175.
[22] H. Li, X. Zhang, Y. Huo, J. Zhu, Environ. Sci. Technol 41 (2007) 4410.
[23] K. Yang, Y. Dai, B. Huang, Phys. Rev. B 76 (2007) 195201.
[24] K. Yang, Y. Dai, B. Huang, J. Phys. Chem. C 111 (2007) 18985.
[25] K. Tan, H. Zhang, C. Xie, H. Zheng, Y. Gu, W.F. Zhang, Catal. Commun. 11 (2010) 331.
[26] L. Jia, C. Wu, Y. Li, S. Han, Z. Li, B. Chi, J. Pu, L. Jian, Appl. Phys. Lett. 98 (2011) 211903.
[27] Y. Lin, Z. Jiang, X. Hu, X. Zhang, J. Fan, Appl. Phys. Lett. 100 (2012) 102105.
[28] B.J. Morgan, G.W. Watson, J. Phys. Chem. C 114 (2010) 2321.
[29] J. Stausholm-Møller, H.H. Kristoffersen, B. Hinnemann, G.K.H. Madsen, B. Hammer, J. Chem. Phys. 133 (2010) 144708.
[30] L. Jia, C. Wu, S. Han, N. Yao, Y. Li, Z. Li, B. Chi, J. Pu, L. Jian, J. Alloys Compd. 509 (2011) 6067.
[31] C. Arrouvel, S.C. Parker, M.S. Islam, Chem. Mater. 21 (2009) 4778.

[32] A. Jedidi, A. Markovits, C. Minot, S. Bouzriba, M. Abderraba, Langmuir 26 (2010) 16232.
[33] Y.G. Zhang, Y.X. Wang, J. Appl. Phys. 110 (2011) 033519.
[34] W. Chen, P. Yuan, S. Zhang, Q. Sun, E. Liang, Y. Jia, Physica B 407 (2012) 1038.
[35] Y. Ma, J. Zhang, B. Tian, F. Chen, L. Wang, J. Hazard. Mater. 182 (2010) 386.
[36] G. Kresse, J. Hafner, J. Phys. Rev. B 47 (1994) 558.
[37] G. Kresse, J. Furthmüller, J. Phys. Rev. B 54 (1996) 11169.
[38] J.P. Perdew, C.J. Ahevary, S.H. Vosko, K.A. Jackson, M.R. Pederson, D.J. Singh, C. Fiolhais, Phys. Rev. B 46 (2004) 6671.
[39] H.J. Monkhorst, J.D. Pack, Phys. Rev. B 13 (1976) 5188.
[40] S.L. Dudarev, G.A. Botton, S.Y. Savarsov, C.J. Humphreys, A.P. Sutton, Phys. Rev. B 57 (1998) 1505.
[41] K. Yang, Y. Dai, B. Huang, Y.P. Feng, Phys. Rev. B 81 (2010) 033202.
[42] K. Yang, Y. Dai, B. Huang, M.H. Whangbo, J. Phys. Chem. C 113 (2009) 2624.
[43] M.E. Arroyo-de Dompablo, A. Morales-Garca, M. Taravillo, J. Chem. Phys. 135 (2011) 054503.
[44] M.Y. Kuo, C.L. Chen, C.Y. Hua, H.C. Yang, P. Shen, J. Phys. Chem. B 109 (2005) 8693.
[45] J. Lee, J. Park, J. Cho, Appl. Phys. Lett. 87 (2005) 011904.
[46] C.D. Valentin, G. Pacchioni, A. Selloni, Phys. Rev. B 70 (2004) 085116.
[47] K. Yang, Y. Dai, B. Huang, J. Phys. Chem. C 111 (2007) 12086.
[48] R. Shirley, M. Kraft, O.R. Inderwildi, Phys. Rev. B 81 (2010) 075111.